

Mitigating Ambiguities in 3D Classification with Gaussian Splatting*

Ruiqi Zhang^{1,†}, Hao Zhu^{1,†}, Jingyi Zhao², Qi Zhang³, Xun Cao^{1,*}, Zhan Ma^{1,*}

¹ Nanjing University, ² Imperial College London, ³ Vivo Company

† Equal contribution. * Corresponding author: {caoxun, mazhan}@nju.edu.cn

Abstract

3D classification with point cloud input is a fundamental problem in 3D vision. However, due to the discrete nature and the insufficient material description of point cloud representations, there are ambiguities in distinguishing wire-like and flat surfaces, as well as transparent or reflective objects. To address these issues, we propose Gaussian Splatting (GS) point cloud-based 3D classification. We find that the scale and rotation coefficients in the GS point cloud help characterize surface types. Specifically, wire-like surfaces consist of multiple slender Gaussian ellipsoids, while flat surfaces are composed of a few flat Gaussian ellipsoids. Additionally, the opacity in the GS point cloud represents the transparency characteristics of objects. As a result, ambiguities in point cloud-based 3D classification can be mitigated utilizing GS point cloud as input. To verify the effectiveness of GS point cloud input, we construct the first real-world GS point cloud dataset in the community, which includes 20 categories with 200 objects in each category. Experiments not only validate the superiority of GS point cloud input, especially in distinguishing ambiguous objects, but also demonstrate the generalization ability across different classification methods.

1. Introduction

“The performance of machine learning methods is heavily dependent on the choice of data representation (or features) on which they are applied.” Bengio et al. [1]

3D classification, which aims at identifying and categorizing objects with 3D point cloud input, is gaining increasing attention due to the convenience of 3D acquisition equipment and its better ability to characterize structure and handle occlusions compared to traditional 2D images. Different from the regular grids in 2D images, the 3D point cloud is organized in an irregular, unordered way, leading to the development of various neural network ar-

*The work was supported in part by the National Key Research and Development Project of China (2022YFF0902402) and NSFC (Grant 62473193).

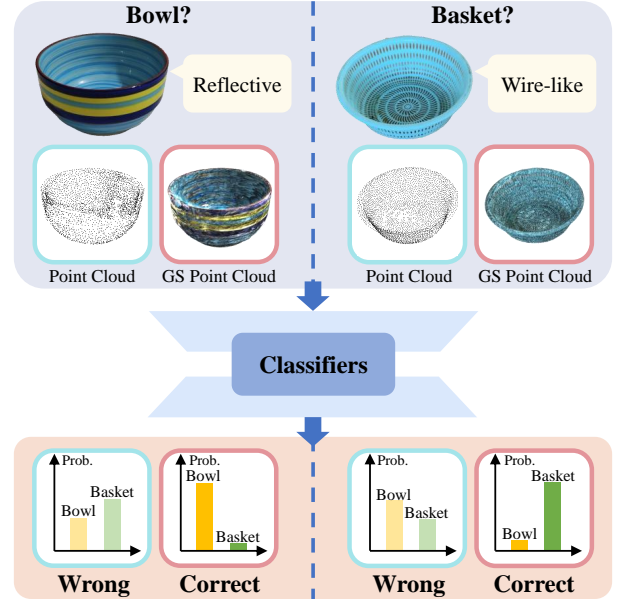


Figure 1. Illustration of ambiguity mitigation in 3D classification using GS point cloud. Although the Bowl and the Basket have different surface types (flat vs wire-like, specular vs diffuse reflection), existing classifiers often confuse them due to similar shapes when described as traditional point cloud, resulting in wrong probability predictions. These ambiguities can be mitigated by introducing GS point cloud.

chitectures [7, 10, 11, 19–21, 27, 30] for extracting local shapes.

However, due to the discrete nature and hard description of existence in point cloud representation, there are two inherent ambiguities in characterizing local shapes and appearance in existing point cloud-based classification methods. For the first ambiguity, the sampling rate of existing 3D acquisitions is often insufficient for characterizing high-frequency structures, resulting in similar point cloud representations for wire-like and flat surfaces of objects that belong to different categories. For the second ambiguity, existing point cloud representation assumes that the components of a 3D object follow a hard existing (1) or non-existing (0) constraint, without any intermediate state,

which violates the description of transparent and reflective objects in the real world. As a result, existing point cloud-based classification methods may struggle to distinguish between objects with wire-like and flat surfaces, as well as those with similar structures but different transparency and reflectivity.

To mitigate the ambiguities in point cloud-based 3D classification, we propose Gaussian Splatting (GS) [8] point cloud-based classification. GS point cloud is originally designed for rendering realistic images of novel views with a set of images captured from different positions. To achieve this goal, particularly in compensating for holes caused by occlusion and modeling transparent or reflective objects, each 3D point is represented as a continuous 3D Gaussian kernel function, with an additional opacity coefficient to characterize each point’s soft existence. We note that the incorporation of these GS coefficients compensates for the coarse shape representation in point cloud, thereby enhancing the accuracy of classification models. Fig. 1 illustrates that integrating GS point cloud effectively mitigates ambiguities in 3D classification.

To verify the efficacy of GS point cloud in 3D classification, we build the first large-scale real-world dataset in the community based on an existing multi-view image dataset [34]. The proposed dataset contains 4,000 objects from 20 categories, including easily misclassified objects such as the wire-like, flat, and reflective objects mentioned above. On this basis, several classical and state-of-the-art classification methods are used for comparison, where only the network input is replaced from pure point cloud (*i.e.*, position) to GS point cloud (*i.e.*, position, standard deviations, rotation matrix, and opacity), while other network components remain unchanged. We find that the introduction of Gaussian coefficients significantly improves classification for ambiguous objects such as Loudspeaker and Paper box (with similar cuboid structures but different wire-like and flat surfaces, respectively), and Mug and Ashcan (with similar structures but different reflectivity). Furthermore, by visualizing the global features in these neural networks using the t-SNE technique (see Fig. 7), we observe that the separability between different categories is significantly increased, which verifies the effectiveness of the added Gaussian coefficients in GS point cloud for 3D classification. Specifically, the main contributions of the work include,

1. As far as we know, this is the first exploration to enhance 3D task (namely classification) using GS point cloud. We provide a deep analysis of the ambiguities in traditional point cloud-based classification and how GS point cloud mitigates them theoretically.
2. We construct the first large-scale real-world GS point cloud dataset, which provides the data base for various GS point cloud-based 3D tasks in future.
3. Quantitative and qualitative experimental results demon-

strate that the GS point cloud effectively mitigates ambiguities and improves classification accuracy across a wide range of methods.

2. Related Work

2.1. 3D Classification

3D classification with point cloud input has gained significant attention due to the widespread application, advancements in 3D acquisition equipment, and rapid development of deep learning techniques. Four main types of methods have been proposed to process the irregular and unordered structure of point cloud, *i.e.*, the point-wise MLP, convolution-based, graph-based, and hierarchical data structure-based methods. The first method [16, 19–21] applies multiple shared Multi-Layer Perceptrons (MLPs) to extract features from the input point cloud matrix, then these features are aggregated. The second method [10, 13, 14, 24] designs specific convolution operators to connect neighboring points in 3D space. By iteratively applying these operators, deep features are obtained for further analysis. The third method [7, 22, 28] treats point cloud as a graph, where each point is a graph’s vertex and direct edges are built between neighboring points, then a graph neural network is applied. The fourth method [9, 11, 12] organizes the point cloud into hierarchical structures, where deep features are extracted from leaf nodes to the root node hierarchically.

Although numerous methods have been proposed, the inherent ambiguities in point cloud representation for classifying wire-like, flat surfaces, and transparent or reflective objects remain unaddressed.

2.2. 3D Gaussian Splatting

GS [8] is an emerging technique for novel view synthesis build on point cloud-based rendering. To overcome the limitations of pure point cloud for representing view-dependent textures of 3D objects, opacity and spherical harmonics [33] are attached to each point’s attributes. However, due to the discrete nature of point cloud, there are many holes in the rendered image. To address this issue, each point is modeled using a 3D anisotropic Gaussian function. This allows the textures of empty spaces to be represented, effectively mitigating the holes problem.

Due to the high-quality reconstruction and high-efficiency rendering, GS dominates the area of novel view synthesis and has been further optimized by subsequent research. Mip-Splatting [35] constrains the frequency content of 3D representations to below half the maximum sampling frequency, effectively mitigating high-frequency artifacts resembling Gaussian shapes. Scaffold-GS [15] initializes a voxel grid with learnable features assigned to each voxel point, where the attributes of the Gaussians are de-

rived from interpolated features and lightweight neural networks, resulting in more accurate view-dependent effects while reducing the model’s storage. HAC [4] builds upon the concept of Scaffold-GS [15] by representing the scene using anchor points, each associated with learnable features. Additionally, it introduces an adaptive quantization module that compresses the anchor point features through a multi-resolution hash grid [17].

However, to the best of the authors knowledge, existing works mainly focus on improving the rendering quality or efficiency of GS, and none of them think deeply on how this new representation can empower traditional computer vision tasks. Compared with these works, we build the first large-scale real-world GS dataset for classification and provide a deep analysis both qualitatively and quantitatively.

3. GS Point Cloud-based 3D Classification

In this section, we first introduce the background of GS point cloud representation. Next, we describe the pipeline used throughout the paper of 3D classification with both point cloud and GS point cloud inputs. Finally, we analyze the advantages of GS point cloud-based classification for mitigating ambiguities.

3.1. GS Point Cloud

Given a 3D object, traditional point cloud represents it using multiple isolated points and records each point’s position $\mathbf{p} = [x, y, z]^\top$ and color $\mathbf{c} = [r, g, b]^\top$. GS point cloud differs from traditional one by treating the object as a combination of multiple 3D Gaussian distributions. As a result, more information for characterizing the Gaussian distribution is recorded, namely, the standard deviation $\mathbf{s} = [s_x, s_y, s_z]^\top$ along three axes and the rotations around the axes. Note that, because the standard deviation is also called scale in GS-related papers, these two terms are used interchangeably in the following sections. The quaternion $\mathbf{q} = [q_1, q_2, q_3, q_4]^\top$ is widely used here to represent rotation, as it avoids ambiguities associated with Euler angle representation. Additionally, GS point cloud softens the opacity $\mathbf{o} \in [0, 1]$ to describe the material features of each point, unlike the constant $\mathbf{o} = 1$ in traditional point cloud. Finally, GS point cloud extends the pure color to a color function, *i.e.*, a series of spherical harmonics, for characterizing view-dependent colors.

3.2. Pipeline of 3D Classification

A point cloud can be represented as $(\mathbf{P} \triangleq \{\mathbf{p}_i\}_{i=1}^N, \mathbf{y})$, where $\mathbf{p}_i = [x, y, z]^\top$ represents the coordinate of the i -th point and N is the total number of points in the cloud. The ground-truth label $\mathbf{y} \in \{1, 2, \dots, k\}$ indicates one of k possible classes. Given such a point cloud, classical

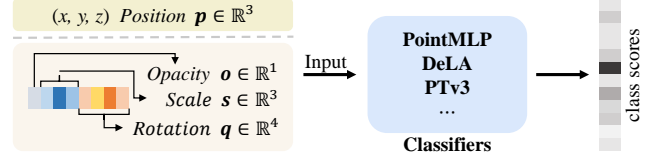


Figure 2. Pipeline of 3D classification used throughout the paper.

learning-based classification methods $\mathbf{F}_\theta(\cdot)$ take the coordinates $\{\mathbf{p}_i\}_{i=1}^N$ as input. The output is the probability distribution over k categories,

$$\mathbf{F}_\theta(\mathbf{P}) \triangleq \{F_{\theta,j}\}_{j=1}^k, \quad (1)$$

where $F_{\theta,j}$ is the probability belonging to the j -th class. To supervise the training of parameters θ in the classification model, the cross-entropy loss function between $\mathbf{F}_\theta(\mathbf{P})$ and \mathbf{y} is often used.

For GS point cloud-based classification, we adopt the traditional point cloud-based classification pipeline, modifying only the input to include GS coefficients. Although GS point cloud has multiple coefficients, we use only four here, *i.e.*, position, standard deviation, rotation, and opacity, namely, $(\mathbf{P}_{GS} \triangleq \{\mathbf{p}_i, \mathbf{o}_i, \mathbf{s}_i, \mathbf{q}_i\}_{i=1}^N, \mathbf{y})$. Note that spherical harmonics are excluded to ensure a fair comparison, as traditional point cloud do not include color attributes. Fig. 2 visualizes the pipeline of 3D classification used throughout the paper.

3.3. Mitigating Ambiguities in 3D Classification

Considering the discrete nature and hard description of existence in point cloud representation, there are two main ambiguities in characterizing local shapes and appearances in point cloud-based classification methods. The first ambiguity arises from the insufficient sampling rate of point cloud, making it difficult to accurately capture local geometric structures and surface details of objects. This can lead to inconsistencies in the classification results when dealing with objects that have similar global shapes but different local features, such as the wire-like and flat surfaces. The second ambiguity in appearance-related characterization is caused by the hard existing constraint in point cloud, resulting in representation that struggles to differentiate objects with similar structures but varying transparency and reflectivity. These ambiguities limit the performance of existing classifiers in distinguishing objects with similar structures but different local shapes and material properties.

According to the definition mentioned in Sec. 3.2, the GS-based point cloud representation can mitigate the ambiguities of traditional point cloud-based classification in two aspects,

1. **Ambiguity in local shape characterization.** Due to the discrete nature of traditional point cloud, there is an ambiguity in distinguishing the wire-like surfaces from flat

ones due to the lack of information about the local geometry. In contrast, GS-based point cloud offers a continuous representation, where each GS point not only describes its own position but also encodes information about its neighboring space. By representing the point cloud as Gaussian ellipsoids, where the covariance matrix defines the scale and rotation of each ellipsoid, the GS-based classification provides a more robust and accurate description of local shapes, effectively addressing the first ambiguity. As shown in Fig. 3, the scale controls the size of the ellipsoid, while the rotation determines its orientation, and together they describe the local geometry of the surface. For example, the wire-like surface in Fig. 3(b) is often represented by multiple slender ellipsoids, while flat surfaces like Fig. 3(a) are represented by a small number of broader, flat ellipsoids. Consequently, the GS-based framework classifies them by constructing a continuous representation of the point cloud, which captures both the global and local geometric features of objects, allowing for a more discriminative classification.

2. Ambiguity in appearance-related characterization.

In traditional point cloud representation, each coordinate refers to an opaque point in 3D space, resulting in ambiguity when distinguishing objects with similar shapes but different transparency. GS point cloud softens this constraint by relaxing the constant opacity of 1 to a variable opacity in the range $[0, 1]$. Comparing Fig. 3(a) and Fig. 3(c) reveals that although the metal box and glass container share similar flat surfaces and exhibit comparable point cloud distributions, the GS point cloud effectively differentiates these surface types by representing scene transparency through opacity. This capability enhances 3D classification for transparent or reflective objects, providing greater clarity and consistency in point cloud data, and enabling more accurate classification.

4. Experiments

The previous section has explained the effectiveness of additional coefficients of GS point cloud for 3D classification in theory. In this section, we focus on validating these analyses through experiments.

4.1. Experiments Setup

Dataset. Existing point cloud datasets [2, 25, 31, 34] provide only 3D positions and lack coefficients related to GS, making them unsuitable for our task. To validate the effectiveness of GS point cloud, we build the first large-scale real-world GS point cloud dataset, based on the MImageNet dataset [34]. MImageNet consists of 219,188 objects from 238 classes, where each object is represented by multi-view images and their corresponding binary masks. Using the official GS implementation [8], we

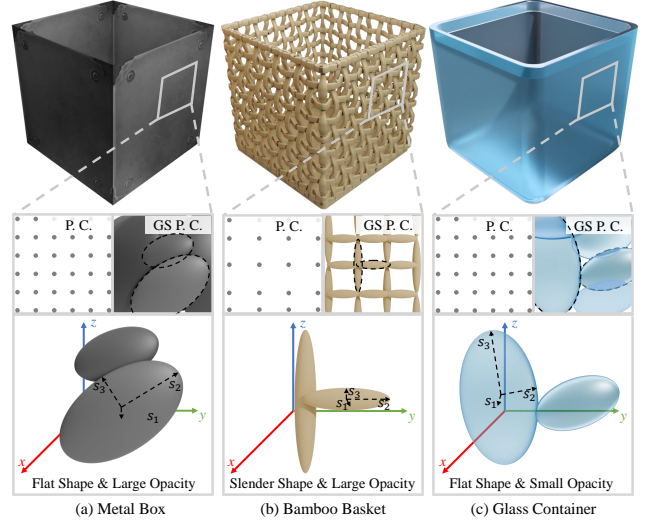


Figure 3. Comparison between point cloud and the ellipsoid representation in Gaussian Splatting (GS). These three examples illustrate how opacity, scale, and rotation of Gaussian coefficients represent object transparency and surface structure. In the left example, a series of large, flat ellipsoids with high opacity represent the flat, opaque surface of the metal box. In the middle example, adjustments in scale and rotation enable ellipsoids to follow the intricate, wire-like structure of the bamboo basket. The right example uses low-opacity, flat ellipsoids to represent the smooth, transparent surface of the glass container.

generate GS point cloud from multi-view images. However, view-specific masks frequently introduce inconsistencies between views, as they are generated independently by a third-party segmentation method [18]. These inconsistencies degrade the quality of the reconstructed GS point cloud, complicating 3D classification evaluation. To address these challenges, we manually curated a subset of 4,000 objects, selecting 20 categories from the initial set of 238, with 200 examples per category. Each object was associated with approximately 30 masks, a labor-intensive process requiring careful attention to ensure consistency across views. We structured the data meticulously and performed object-by-object training, which took over 600 GPU hours on a single A100 card.

Our GS point cloud dataset stands out from traditional point cloud datasets by providing local structure characterization that captures finer geometric details in the scene through scale and rotation embedded in each point, as well as transparency characterization that conveys information about an object’s transparency and reflectivity. While our research focuses on point-based classification and does not incorporate texture-related spherical harmonics, our dataset retains these coefficients. Compared to traditional point cloud rendering, our GS point cloud dataset enables high-fidelity, view-dependent image rendering, which significantly facilitates multiview-based classification meth-

Dataset	# of objects	# of categories	Real	Local Structure Characterization	Transparency Characterization	View-dependent Color
ShapeNet [2]	51k	55	✗	✗	✗	✗
ModelNet [31]	12k	40	✗	✗	✗	✗
ScanObjectNN [25]	14k	15	✓	✗	✗	✗
MVPNet [34]	87k	150	✓	✗	✗	✗
GS dataset (ours)	4k	20	✓	✓	✓	✓

Table 1. Comparison of other point cloud datasets with our proposed GS point cloud dataset.

Method	w/o. GS coeffs.		w. GS coeffs.	
	OA (%)	mAcc (%)	OA (%)	mAcc (%)
PointNet	73.56	73.77	80.87 (+7.31)	81.46 (+7.69)
PointNet++	83.02	82.17	86.63 (+3.61)	86.18 (+4.01)
PointNeXt	87.77	86.54	89.78 (+2.01)	88.70 (+2.16)
PointMLP	87.91	86.75	90.21 (+2.30)	89.48 (+2.73)
DeLA	88.78	87.92	90.36 (+1.58)	89.41 (+1.49)
PTv3	88.78	87.88	89.93 (+1.15)	88.46 (+0.58)

Table 2. Comparison of overall accuracy and mean accuracy for different baseline methods before and after incorporating Gaussian coefficients.

ods [5, 6, 23, 29, 32], enhancing the classification of real-world objects with diverse material properties.

Baseline Algorithms. In our experiments, we select a set of representative point-based methods for validation. These include the groundbreaking PointNet [19] and PointNet++ [20], which process point cloud using point-wise MLP. Additionally, we compare state-of-the-art methods developed upon PointNet/PointNet++, such as PointNeXt [21], which enhances performance through an optimized training strategy, and PointMLP [16], which significantly boosts inference speed with a lightweight local geometry extractor. Finally, we also consider state-of-the-art methods from other categories, including convolution-based approaches like DeLA [3] and transformer-based methods such as PTv3 [30], both of which have achieved impressive results in their respective domains.

In implementation, all results are obtained by re-training the official codes and following official guidelines released by authors with a 24G 3090 GPU. All of these methods are combined with both traditional point cloud and GS point cloud inputs. When verifying the effectiveness of GS point cloud input, we modifies only the first layer of the network to accommodate the increased channels, *i.e.*, from 3 (only position) to 4 (position+opacity), 10 (position+scale+rotation), 11 (position+opacity+scale+rotation).

4.2. Results

Tab. 2 provides a comprehensive comparison of the overall accuracy (OA) and the mean class accuracy (mAcc) across different methods, both with and without GS coefficients.

As observed, all methods show an improvement in both OA and mAcc when GS point cloud is employed. For earlier works such as PointNet, the integration of GS coefficients leads to a notable improvement of over 7% in both metrics. In contrast, the state-of-the-art methods, including PointNeXt, PointMLP, DeLA, and PTv3, also demonstrate improvements, although to a lesser extent. The OA for these methods reaches approximately 90%, with the minimum improvement being 1% over the raw point cloud inputs.

To further analyze the effectiveness of different coefficients in GS point cloud, we feed the combinations of position+opacity (*po*), position+scale+rotation (*psq*) and position+opacity+scale+rotation (*posq*) into existing networks, respectively. Tab. 3 provides detailed classification probabilities of the correct class by PointNet for different categories, where the probabilities have increased to varying degrees. Fig. 4 shows the evolution of probability distribution with different inputs. A more detailed explanation of Tab. 3 and Fig. 4 will be provided in the following sections.

4.3. Opacity

According to Tab. 3, the introduction of opacity significantly improves classification accuracy for objects with reflective or transparent properties, such as the Train, Mug, and Bowl. Fig. 4 visualizes these improvements. In the red rectangle of Fig. 4(a), the probability of correctly classifying the Train increases (*i.e.*, from orange to red in the 3-rd row and 3-rd col block), while the probability of misclassification as the Pipe is also reduced (*i.e.*, the 3-rd row and 20-th col block). The first row of Fig. 5 visualizes the comparisons. It is observed that the shape of the Train is similar to the Pipe, *i.e.*, both are strip-like objects. However, the Train is designed with a streamlined structure to reduce wind resistance, giving it a glossy surface with a lower opacity value. In contrast, the Pipe is typically made of plastic, which exhibits low reflectivity, resulting in an opacity value close to 1. As a result, the Train and the Pipe are classified more accurately when the additional opacity coefficient is added to the position.

Apart from the Train and the Pipe, it is also difficult to distinguish the Mug from the Ashcan if only the position is used. In Tab. 3, when only position is used, the probability of correctly classifying the Mug is only 0.46. One

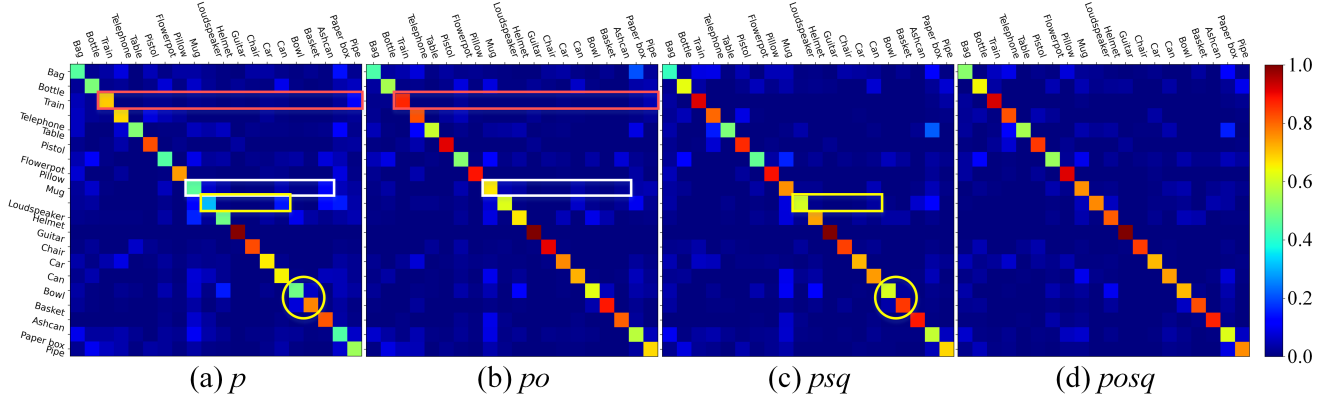


Figure 4. Comparisons of the probabilities output from the PointNet with different inputs. From left to right: only position, position+opacity, position+scale+rotation, position+opacity+scale+rotation. For each sub-figure, the color of the i -th row and j -th col represents the probability of the i -th object be classified as the j -th one. The rightmost image is the colorbar.

GS inputs		Bag	Bottle	Train	Telephone	Table	Pistol	Flowerpot	Pillow	Mug	Loudspeaker
Prob.	p	0.45	0.50	0.69	0.67	0.51	0.82	0.45	0.74	0.46	0.31
	po	0.44	0.55	0.86	0.82	0.59	0.91	0.51	0.88	0.66	0.62
	psq	0.41	0.63	0.91	0.79	0.50	0.86	0.47	0.89	0.75	0.60
	$posq$	0.51	0.64	0.92	0.82	0.55	0.84	0.53	0.91	0.75	0.76
GS inputs		Helmet	Guitar	Chair	Car	Can	Bowl	Basket	Ashcan	Paper box	Pipe
Prob.	p	0.48	0.99	0.82	0.65	0.65	0.48	0.76	0.81	0.44	0.54
	po	0.66	0.99	0.90	0.76	0.72	0.62	0.88	0.80	0.57	0.67
	psq	0.73	0.99	0.84	0.71	0.74	0.61	0.85	0.88	0.58	0.68
	$posq$	0.80	0.99	0.84	0.71	0.74	0.71	0.82	0.87	0.61	0.75

Table 3. The average probability of the correct class obtained by PointNet for each category with different inputs.

of the main reasons is the similar structure to the Ashcan. As demonstrated in the second row of Fig. 5, both the Mug and the Ashcan have a concave surface, which causes the model to have difficulty distinguishing them based on position alone. Although the Mug has a handle, PointNet assigns a higher probability to classifying it as the Ashcan rather than the correct category, Mug. Introducing opacity to the network significantly reduces this misclassification. As shown in the white rectangles in Fig. 4(a) and Fig. 4(b), the probability of correctly classifying the Mug improves significantly (*i.e.*, from green to yellow in the 9-th row and 9-th col block), and the probability of misclassifying it as the Ashcan is also reduced (*i.e.*, the 9-th row and 18-th col block). The change of the histogram in the second row of Fig. 5 also verifies the effect of the opacity coefficient.

4.4. Scale and Rotation

By comparing Fig. 4(a) and Fig. 4(c), it is observed that additional scale and rotation coefficients in GS point cloud help in classifying objects with wire-like surfaces as distinct from flat ones. For example, in the yellow rectangles, the probability of correctly classifying the Loudspeaker is sig-

nificantly improved (*i.e.*, from cyan to yellow in the 10-th row and 10-th col block), while the probability of misclassifying it as the Can is reduced (*i.e.*, the 10-th row and 15-th col block). The first row of Fig. 6 visualizes the point cloud and GS representations of the Loudspeaker and the Can. Because the Loudspeaker shares a similar global structure to the Can, *i.e.*, both are cylinder-like objects, it is difficult to distinguish them according to the point cloud (shown in the top-right boxes). As a result, the classifier, when fed with point cloud input, outputs unreliable results.

However, the situation changes when introducing the Gaussian coefficients. As shown in Fig. 6, since the Loudspeaker is designed to amplify the sound, its surface contains many perforations. The GS point cloud represents this wire-like surface structure as multiple disjoint slender Gaussian ellipsoids, with their main axes distributed along the boundaries between neighboring holes. In contrast, the Can, designed to hold goods, has a flat surface without any perforations. This flat surface is represented by several intersecting flat ellipsoids in the GS point cloud. By comparing the Gaussian ellipsoids, it becomes apparent that the structures, originally similar in the point cloud, have be-

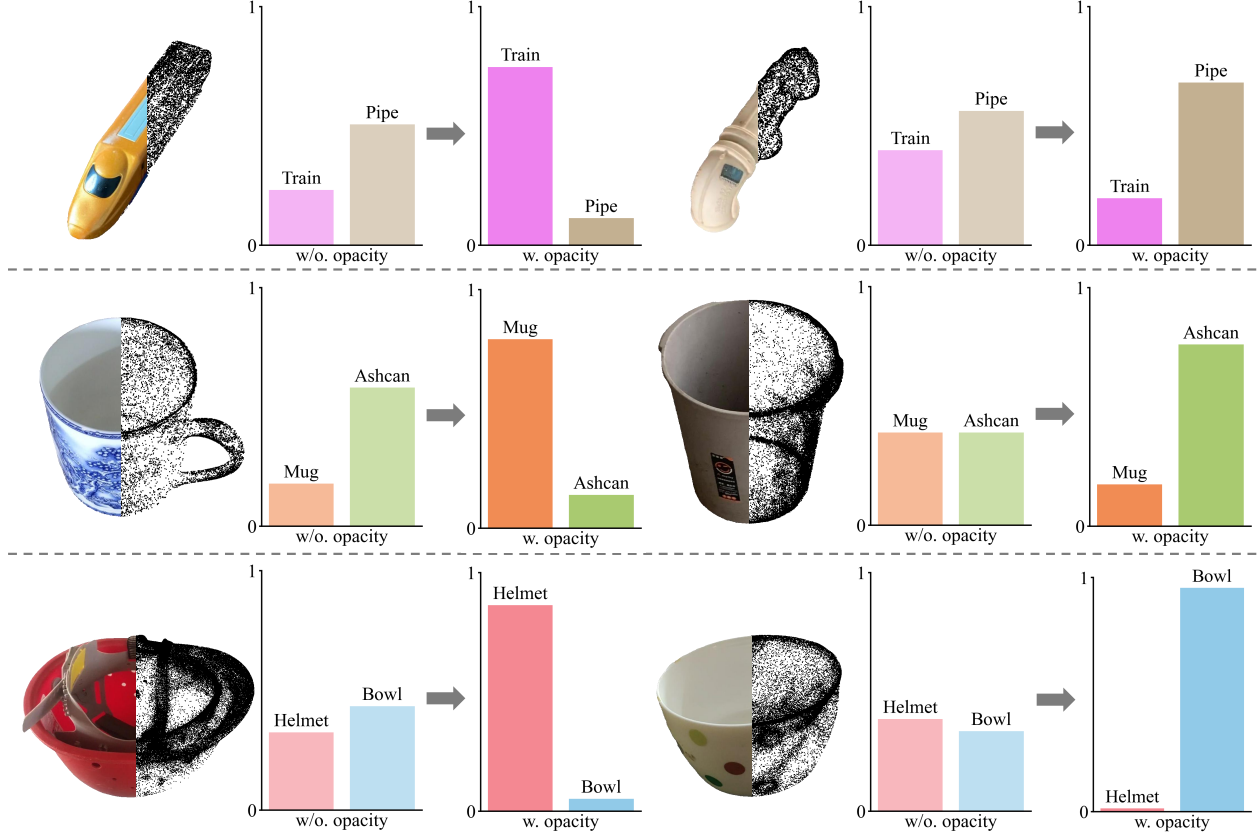


Figure 5. Comparison of the geometric similarity leading to misclassification between the helmet and the bowl (first row), and the classification probability map before and after using opacity, where red represents the correct class and blue represents other classes (second row).

come significantly distinct. As a result, the right classification probabilities for both the Loudspeaker and the Can are both improved when using the GS point cloud.

The improvement brought by the GS point cloud not only exists in the classification of the Loudspeaker and the Can but also appears in classifying other objects with wire-like and flat surfaces such as the Bowl and the Basket (*i.e.*, the yellow cycles in Fig. 4(a) and Fig. 4(c), and the second row in Fig. 6), as well as the Loudspeaker and the Paper box (*i.e.*, the third row in Fig. 6). These improvements validate the theoretical analysis presented in Sec. 3.3.

4.5. Features Visualization

To better understand the effects of different components in GS point cloud-based 3D classification, we focus on the high-dimensional global feature in the point-wise MLP methods (please refer to Fig. 2 of [19, 20] for details). We feed the entire dataset into PointNet and visualize the global feature using the t-SNE (t-Distributed Stochastic Neighbor Embedding) technique [26].

Fig. 7 displays our visualization results, demonstrating the improvement in clustering visualization as we varied the input from only position to include opacity, scale, and rota-

tion, and finally incorporating all Gaussian coefficients. It is evident that with the inclusion of Gaussian-related coefficients, the overlap between different categories in the clustering graph decreases, boundaries become clearer, and instances within the same category are grouped more closely. Using only position information results in greater overlap, especially when dealing with similar shapes. However, when geometric features combined with other Gaussian coefficients are used as input, this overlap is significantly reduced, and different categories are distinctly separated. This phenomenon not only exists in the global feature produced by PointNet, but also appears in other classifiers. For further details, please refer to the supplementary material.

5. Conclusion

In this work, we have proposed the GS point cloud-based 3D classification. We have identified two inherent ambiguities in traditional point cloud-based 3D classification, *i.e.*, the characterization of local shape and appearance. These ambiguities are independent of the subsequent classification models and thus cannot be effectively addressed. The GS point cloud represents 3D objects as Gaussian ellipsoids

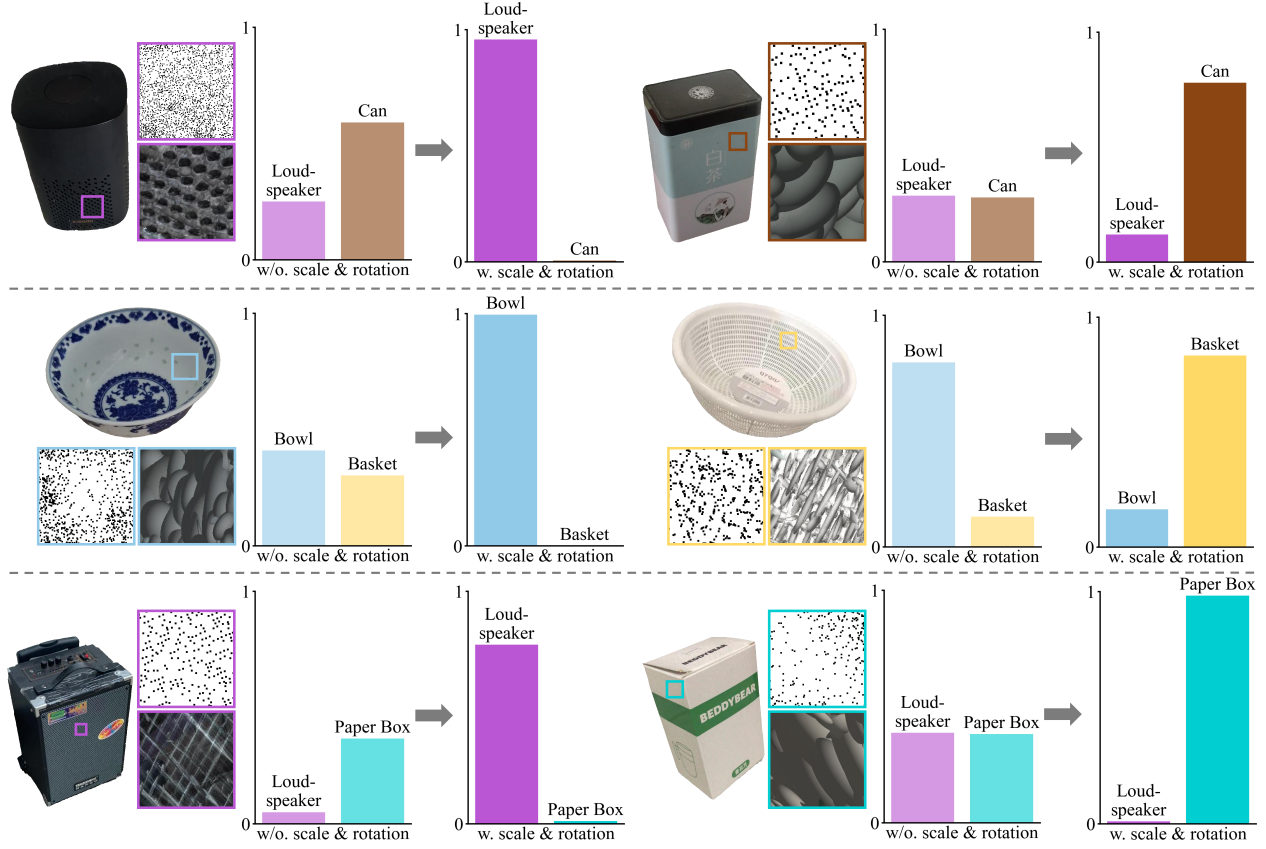


Figure 6. Comparison of the probability of obtaining the correct category with or without using the scale and orientation of the GS point cloud. For each object, the right-top and right-bottom images visualize the point cloud and GS point cloud of the zoom-in area box. Two histograms right are the classification probabilities output from the PointNet without and with the scale and rotation coefficients in GS point cloud.

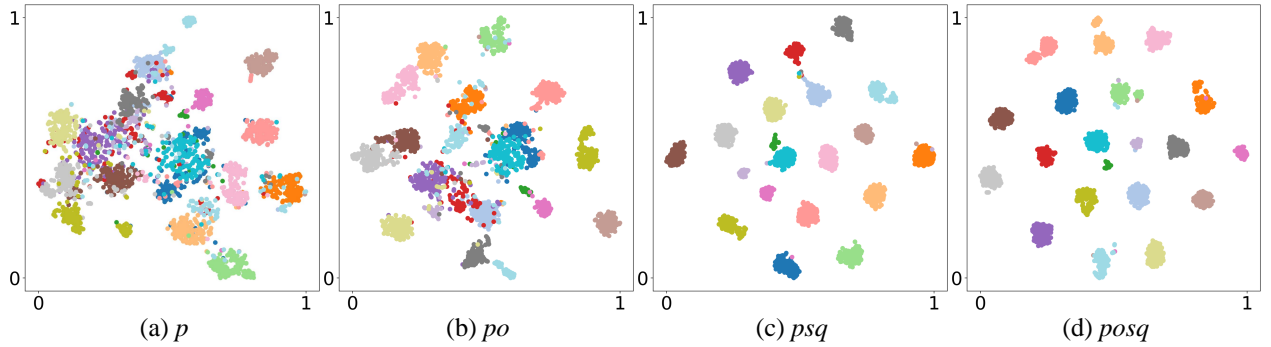


Figure 7. Visualizations of the global features in PointNet with different inputs using t-SNE technique. (a)-(d) are visualized features of network with only position, position+opacity, position+scale+rotation and position+opacity+scale+rotation inputs, respectively.

with transparency, where the scale, rotation, and opacity of the ellipsoids better characterize the object’s local shapes and appearance, significantly mitigating these ambiguities. We have demonstrated the enhancement of the GS point cloud and its improvements in object classification, addressing the aforementioned ambiguities, using the first GS point cloud dataset we constructed.

Unlike traditional point cloud, which can be captured with a variety of devices, the acquisition of GS point cloud relies on multiple RGB cameras, thereby limiting its applicability to a broader range of 3D tasks. Consequently, it is necessary to develop new devices and algorithms for obtaining GS point cloud in the future.

References

- [1] Yoshua Bengio, Aaron Courville, and Pascal Vincent. Representation learning: A review and new perspectives. *IEEE Transactions on Pattern Analysis and Machine Intelligence*, 35(8):1798–1828, 2013. 1
- [2] Angel X. Chang, Thomas Funkhouser, Leonidas Guibas, Pat Hanrahan, Qixing Huang, Zimo Li, Silvio Savarese, Manolis Savva, Shuran Song, Hao Su, Jianxiong Xiao, Li Yi, and Fisher Yu. ShapeNet: An Information-Rich 3D Model Repository. Technical Report arXiv:1512.03012 [cs.GR], Stanford University — Princeton University — Toyota Technological Institute at Chicago, 2015. 4, 5
- [3] Binjie Chen, Yunzhou Xia, Yu Zang, Cheng Wang, and Jonathan Li. Decoupled local aggregation for point cloud learning. *arXiv preprint arXiv:2308.16532*, 2023. 5
- [4] Yihang Chen, Qianyi Wu, Weiyao Lin, Mehrtash Harandi, and Jianfei Cai. Hac: Hash-grid assisted context for 3d gaussian splatting compression. In *European Conference on Computer Vision*, 2024. 3
- [5] Yifan Feng, Zizhao Zhang, Xibin Zhao, Rongrong Ji, and Yue Gao. Gvcnn: Group-view convolutional neural networks for 3d shape recognition. In *Proceedings of the IEEE conference on computer vision and pattern recognition*, pages 264–272, 2018. 5
- [6] Abdullah Hamdi, Silvio Giancola, and Bernard Ghanem. Mvtn: Multi-view transformation network for 3d shape recognition. In *Proceedings of the IEEE/CVF International Conference on Computer Vision*, pages 1–11, 2021. 5
- [7] Kaveh Hassani and Mike Haley. Unsupervised multi-task feature learning on point clouds. In *Proceedings of the IEEE/CVF International Conference on Computer Vision*, pages 8160–8171, 2019. 1, 2
- [8] Bernhard Kerbl, Georgios Kopanas, Thomas Leimkühler, and George Drettakis. 3d gaussian splatting for real-time radiance field rendering. *ACM Transactions on Graphics*, 42(4), 2023. 2, 4
- [9] Roman Klokov and Victor Lempitsky. Escape from cells: Deep kd-networks for the recognition of 3d point cloud models. In *Proceedings of the IEEE international conference on computer vision*, pages 863–872, 2017. 2
- [10] Shiyi Lan, Ruichi Yu, Gang Yu, and Larry S Davis. Modeling local geometric structure of 3d point clouds using geocnn. In *Proceedings of the IEEE/cvf conference on computer vision and pattern recognition*, pages 998–1008, 2019. 1, 2
- [11] Huan Lei, Naveed Akhtar, and Ajmal Mian. Octree guided cnn with spherical kernels for 3d point clouds. In *Proceedings of the IEEE/CVF Conference on Computer Vision and Pattern Recognition*, pages 9631–9640, 2019. 1, 2
- [12] Jiaxin Li, Ben M Chen, and Gim Hee Lee. So-net: Self-organizing network for point cloud analysis. In *Proceedings of the IEEE conference on computer vision and pattern recognition*, pages 9397–9406, 2018. 2
- [13] Yongcheng Liu, Bin Fan, Gaofeng Meng, Jiwen Lu, Shiming Xiang, and Chunhong Pan. Densepoint: Learning densely contextual representation for efficient point cloud processing. In *Proceedings of the IEEE/CVF international conference on computer vision*, pages 5239–5248, 2019. 2
- [14] Yongcheng Liu, Bin Fan, Shiming Xiang, and Chunhong Pan. Relation-shape convolutional neural network for point cloud analysis. In *Proceedings of the IEEE/CVF conference on computer vision and pattern recognition*, pages 8895–8904, 2019. 2
- [15] Tao Lu, Mulin Yu, Linning Xu, Yuanbo Xiangli, Limin Wang, Dahua Lin, and Bo Dai. Scaffold-gs: Structured 3d gaussians for view-adaptive rendering. In *Proceedings of the IEEE/CVF Conference on Computer Vision and Pattern Recognition*, pages 20654–20664, 2024. 2, 3
- [16] Xu Ma, Can Qin, Haoxuan You, Haoxi Ran, and Yun Fu. Rethinking network design and local geometry in point cloud: A simple residual MLP framework. In *International Conference on Learning Representations*, 2022. 2, 5
- [17] Thomas Müller, Alex Evans, Christoph Schied, and Alexander Keller. Instant neural graphics primitives with a multiresolution hash encoding. *ACM transactions on graphics (TOG)*, 41(4):1–15, 2022. 3
- [18] Open Source Project. *CarveKit - image-background-remove-tool*. 4
- [19] Charles R Qi, Hao Su, Kaichun Mo, and Leonidas J Guibas. Pointnet: Deep learning on point sets for 3d classification and segmentation. In *Proceedings of the IEEE conference on computer vision and pattern recognition*, pages 652–660, 2017. 1, 2, 5, 7
- [20] Charles Ruizhongtai Qi, Li Yi, Hao Su, and Leonidas J Guibas. Pointnet++: Deep hierarchical feature learning on point sets in a metric space. *Advances in neural information processing systems*, 30, 2017. 5, 7
- [21] Guocheng Qian, Yuchen Li, Houwen Peng, Jinjie Mai, Hasan Hammoud, Mohamed Elhoseiny, and Bernard Ghanem. Pointnext: Revisiting pointnet++ with improved training and scaling strategies. In *Advances in Neural Information Processing Systems (NeurIPS)*, 2022. 1, 2, 5
- [22] Yiru Shen, Chen Feng, Yaoqing Yang, and Dong Tian. Mining point cloud local structures by kernel correlation and graph pooling. In *Proceedings of the IEEE conference on computer vision and pattern recognition*, pages 4548–4557, 2018. 2
- [23] Hang Su, Subhransu Maji, Evangelos Kalogerakis, and Erik Learned-Miller. Multi-view convolutional neural networks for 3d shape recognition. In *Proceedings of the IEEE international conference on computer vision*, pages 945–953, 2015. 5
- [24] Hugues Thomas, Charles R Qi, Jean-Emmanuel Deschaud, Beatriz Marcotequi, François Goulette, and Leonidas J Guibas. Kpconv: Flexible and deformable convolution for point clouds. In *Proceedings of the IEEE/CVF international conference on computer vision*, pages 6411–6420, 2019. 2
- [25] Mikaela Angelina Uy, Quang-Hieu Pham, Binh-Son Hua, Duc Thanh Nguyen, and Sai-Kit Yeung. Revisiting point cloud classification: A new benchmark dataset and classification model on real-world data. In *International Conference on Computer Vision (ICCV)*, 2019. 4, 5
- [26] Laurens van der Maaten and Geoffrey Hinton. Visualizing data using t-sne. *Journal of Machine Learning Research*, 9(86):2579–2605, 2008. 7

- [27] Peng-Shuai Wang. Octformer: Octree-based transformers for 3d point clouds. *ACM Transactions on Graphics (TOG)*, 42(4):1–11, 2023. [1](#)
- [28] Yue Wang, Yongbin Sun, Ziwei Liu, Sanjay E Sarma, Michael M Bronstein, and Justin M Solomon. Dynamic graph cnn for learning on point clouds. *ACM Transactions on Graphics (tog)*, 38(5):1–12, 2019. [2](#)
- [29] Xin Wei, Ruixuan Yu, and Jian Sun. View-gcn: View-based graph convolutional network for 3d shape analysis. In *Proceedings of the IEEE/CVF Conference on Computer Vision and Pattern Recognition*, pages 1850–1859, 2020. [5](#)
- [30] Xiaoyang Wu, Li Jiang, Peng-Shuai Wang, Zhijian Liu, Xihui Liu, Yu Qiao, Wanli Ouyang, Tong He, and Hengshuang Zhao. Point transformer v3: Simpler faster stronger. In *Proceedings of the IEEE/CVF Conference on Computer Vision and Pattern Recognition*, pages 4840–4851, 2024. [1](#), [5](#)
- [31] Zhirong Wu, Shuran Song, Aditya Khosla, Fisher Yu, Linguang Zhang, Xiaoou Tang, and Jianxiong Xiao. 3D shapenets: A deep representation for volumetric shapes. In *Proceedings of the IEEE conference on computer vision and pattern recognition*, pages 1912–1920, 2015. [4](#), [5](#)
- [32] Ze Yang and Liwei Wang. Learning relationships for multi-view 3d object recognition. In *Proceedings of the IEEE/CVF international conference on computer vision*, pages 7505–7514, 2019. [5](#)
- [33] Alex Yu, Ruilong Li, Matthew Tancik, Hao Li, Ren Ng, and Angjoo Kanazawa. Plenotrees for real-time rendering of neural radiance fields. In *Proceedings of the IEEE/CVF International Conference on Computer Vision*, pages 5752–5761, 2021. [2](#)
- [34] Xianggang Yu, Mutian Xu, Yidan Zhang, Haolin Liu, Chongjie Ye, Yushuang Wu, Zizheng Yan, Tianyou Liang, Guanying Chen, Shuguang Cui, and Xiaoguang Han. Mvimnet: A large-scale dataset of multi-view images. In *CVPR*, 2023. [2](#), [4](#), [5](#)
- [35] Zehao Yu, Anpei Chen, Binbin Huang, Torsten Sattler, and Andreas Geiger. Mip-splatting: Alias-free 3d gaussian splatting. In *Proceedings of the IEEE/CVF Conference on Computer Vision and Pattern Recognition (CVPR)*, pages 19447–19456, 2024. [2](#)